Supporting Information

Kraft et al. 10.1073/pnas.1116820109

SI Text

Supporting Experimental Methods. ***Particle synthesis. Linear polystyrene spheres.*** Monodisperse linear (not cross-linked) polystyrene spheres of 1.42 μm in diameter were synthesized by dispersion polymerization. For this 126 mL ethanol (200 Proof), 14 mL deionized water, 10 mL styrene (Reagant Plus, Sigma Aldrich), 0.136 g asobisisobutyronitrile (AIBN) and 5.0 g polyvinylpyrrolidone (PVP, K30, $M_w = 40$ kg/mol) were measured into a 200 mL round bottom flask, closed with a rubber septa and sealed with Teflon tape. To commence polymerization, the flask was immersed in a 75 °C oil bath with its axis of rotation at roughly a 60° angle. Polymerization was carried out for 20 h while rotating the flask at 60 rpm.

Cross-linking of the polystyrene spheres. Typically, an aliquot of a 10% w/w linear polystyrene dispersion was washed with methanol and redispersed in 10% w/w aqueous polyvinyl alcohol (PVA, $M_w = 89$–98 kg/mol, 87–89% hydrolized) twice. After a third centrifugation step the pellet was redispersed with 1% w/w aqueous PVA such that the obtained colloidal dispersion had a weight fraction of approximately 20% w/w. For cross-linking the polystyrene particles, a procedure by Kim et al. was followed (1). A swelling emulsion consisting of 1% w/w aqueous PVA solution ($M_w = 89$–98 kg/mol) and 20% v/v styrene containing 1.5% v/v divinylbenzene, 10% v/v TMSPA (3-(trimethoxysilyl) propyl acrylate , Sigma Aldrich) and 2% w/w V65B (2,2′-azodi (2,4′-dimethylvaleronitrile), initiator)) was prepared either by tip sonication (Branson Sonifier 150, speed 8 for 2 min), or by homogenization (UltraTurrax 20, 8000 rpm for 4 min). The volume of the swelling emulsion was chosen such that a swelling ratio of 4 was achieved, where we define the swelling ratio as $S = m_{\mathrm{monomer}}/m_{\mathrm{polymer}}$ (2). Polymerization was carried out for 24 h while rotating in a 70 °C oil bath.

The final cross-linked particles were 2.41 ± 0.04 μm in diameter. During this step, the surface of the particles became corrugated by adsorption of polystyrene particles nucleated during polymerization, as depicted in Fig. S1*B*. The diameter of these secondary particles was roughly 0.18 μm. The dispersions of cross-linked polystyrene spheres were washed by centrifugation and redispersion in 1% w/w aqueous PVA solutions ($M_w =$ 89–98 kg/mol) three times.

Protrusion formation. To obtain smooth protrusions on the cross-linked polystyrene seed particles, the previous step was repeated. A 20% w/w colloidal dispersion of cross-linked polystyrene seed particles (CPS) was swollen with an emulsion consisting of 1% w/w aqueous polyvinyl alcohol solution ($M_w = 89$–98 kg/mol) and styrene containing 1.5% v/v divinylbenzene and 2% w/w V65B. The protrusions formed by phase separation induced by an overswelling of the particles (3) have a smooth surface. They were polymerized by tumbling in an oil bath at 70 °C for 10 h. The volume of the protrusions relative to the seed particles is determined by the swelling ratio S and is continuously tunable. We note here that some batches of cross-linked seed particles produce more than one protrusion, possibly due to an inhomogeneous cross-link network. To obtain monodisperse, uniform particles we proceeded with a batch of seed particles that only yielded one protrusion per particle during this step.

For colloids with protrusions smaller than the seed particles, the seed dispersion was swollen with a 10% w/w emulsion (swelling ratio $S = 2$). The final particles have a protrusion radius of 1.11 ± 0.06 μm (smooth side, polydispersity (pd) 2.9%) and a seed radius of 1.46 ± 0.06 μm (rough side, pd 2.2%). The total length is 4.9 ± 0.12 μm (pd 2.9%). The roughness inducing secondary particles have a diameter of 185 ± 30 nm (pd 16%). A SEM image of the obtained particles is shown in Fig. S1*C*. Furthermore, large rough spheres of radius 1.6 ± 0.1 μm are employed in the experiments.

To fabricate colloids with protrusions larger than the seed particles a 20% w/w swelling emulsion with swelling ratio $S = 4$ was employed. The final anisotropic particles have a protrusion radius of 1.66 ± 0.06 μm (smooth side) and a seed radius of 1.19 ± 0.05 μm (rough side). The total particle length is 4.70 ± 0.15 μm (pd 3.2%). The roughness inducing spheres have a diameter of 182 ± 40 nm (pd 22%). A scanning electron micrograph (SEM) is shown in Fig. S1*E*.

The colloidal dispersion was washed by centrifugation until all secondary nucleated particles were removed. They were redispersed in 0.3% w/w aqueous polyvinyl alcohol solution ($M_w =$ 30–50 kg/mol) to decrease the layer thickness of the steric stabilization. A schematic of the synthesis of polystyrene dimers with a rough and a smooth side is depicted in Fig. S1.

Characterization. Microscopy. Polymerized samples were imaged using a scanning electron microscope (SEM XL FEG 30, Philips). The dried samples of particles were sputter coated with 4 nm platinum/palladium prior to imaging. Light microscopy was performed with a Zeiss Axioplan microscope using an oil immersion lens (NA = 1.4, 100× magnification). Pictures were captured with a Basler scout camera and saved to disk using Streampix.

Dynamic light scattering (DLS). To measure the polymer sizes, DLS was performed with a Malvern Zetasizer ZS at a scattering angle of 173°.

Zetapotential. The surface-, or zetapotential, of the dimers was measured to be $\Psi = 0.6\ k_{\mathrm{B}}T$ by laser Doppler electrophoresis with a Malvern Zetasizer ZS.

Coating of the glass capillaries. To prevent the particles from adsorbing at the glass slide in the presence of depletant, a coating was applied to the glass capillaries (4). For this, a pipette tip was connected to 50 mm borosilicate glass capillaries via elastic tubing and PTFE tape. Successively, 0.5 mL 1 M aqueous KOH (Merck), 0.5 mL millipore water, 0.5 mL 1% w/w aqueous polyethyleneimine (Fluka, $M_w = 60$ kg/mol, 50% aqueous solution), 0.5 mL millipore water, 0.5 mL 1% w/w aqueous dextran sulfate sodium salt (Acros Organics) and 0.5 mL millipore water were run through the capillaries. To remove excess polymer and salt, the capillaries were then placed in Millipore water for 10 mins and dried with nitrogen gas.

Microscope sample preparation. The samples were prepared by mixing of aqueous solution of polymer, colloidal dispersion, 20 mM NaCl (unless stated otherwise), and millipore water. All components contained 7.7 mM sodium azide (extra pure, Acros Organics) to prevent bacterial growth. The colloidal volume fraction was chosen to be 0.3% w/w. For depletion interaction, dextran polymers of $M_w = 110$ kg/mol (Fluka) and $Mw = 500$ kg/mol (Sigma Aldrich) were dissolved in 7.7 mM aqueous sodium azide (NaN_3). After preparation, the samples were filled in the capillaries and sealed with UV sensitive glue onto microscope slides. To prevent sedimentation the microscope samples were rotated at 10 rpm (VWR stage).

Supplementary Computational Methods. ***Effective pair potentials between colloidal spheres with rough or smooth surfaces.*** The colloidal particles with a rough surface are modeled as hard spheres with diameter σ_r at positions $\mathbf{R}_i$ coated with small hard spheres on the colloidal surface. We consider N_c coated particles with orientations $\hat{\omega}_i$ and N_p polymers with diameter σ_p at positions $\mathbf{r}_j$ in a macroscopic volume V at temperature T. The polymer diameter $\sigma_p = 2r_p$ is taken to be twice the radius of gyration r_p. The colloidal particles are described by a pairwise colloid-colloid interaction Hamiltonian $H_{cc} = \Sigma_{i<j}^{N_c}\phi_{cc}(\mathbf{R}_{ij}, \hat{\omega}_i, \hat{\omega}_j)$, a pairwise colloid-polymer Hamiltonian $H_{cp} = \Sigma_{i=1}^{N_c}\Sigma_{j=1}^{N_p}\phi_{cp}(\mathbf{R}_i - \mathbf{r}_j, \hat{\omega}_i)$, and a polymer-polymer Hamiltonian $H_{pp} \equiv 0$ as the polymers are assumed to be ideal. Here we introduced the colloid-colloid pair potential ϕ_{cc} and the colloid-polymer pair potential ϕ_{cp} given by

$$\beta\phi_{cc}(\mathbf{R}_{ij}, \hat{\omega}_i, \hat{\omega}_j) = \begin{cases} \infty & \text{for } \xi(\mathbf{R}_{ij}, \hat{\omega}_i, \hat{\omega}_j) < 0 \\ 0 & \text{otherwise} \end{cases}$$

$$\beta\phi_{cp}(\mathbf{R}_i - \mathbf{r}_j, \hat{\omega}_i) = \begin{cases} \infty & \text{for } \xi(\mathbf{R}_i - \mathbf{r}_j, \hat{\omega}_i) < 0 \\ 0 & \text{otherwise} \end{cases},$$

where $\beta = (k_\mathrm{B}T)^{-1}$ with k_B the Boltzmann constant, and where $\mathbf{R}_{ij} = \mathbf{R}_i - \mathbf{R}_j$, $\xi(\mathbf{R}_{ij}, \hat{\omega}_i, \hat{\omega}_j)$ denotes the surface-to-surface distance between two coated particles, and $\xi(\mathbf{R}_i - \mathbf{r}_j, \hat{\omega}_i)$ is the surface-to-surface distance between a coated particle and a polymer coil. The total interaction Hamiltonian of the system of interest reads $H = H_{cc} + H_{cp}$. The kinetic energy of the polymers and the colloids is not considered here explicitly, as it is trivially accounted for in the classical partition sums to be evaluated below.

We map the binary mixture of coated particles and ideal polymers with interaction Hamiltonian H onto an effective one-component system with Hamiltonian H^{eff} by integrating out the degrees of freedom of the polymer coils. Our derivation follows closely that of ref. (5).

We consider the system in the (N_c, V, z_p, T) ensemble, in which the fugacity $z_p = \Lambda_p^{-3}\exp(\beta\mu_p)$ of the polymer coils is fixed, with Λ_ν the thermal wavelength of species $\nu = c, p$, and with μ_p the chemical potential of the polymers. The thermodynamic potential $F(N_c, V, z_p, T)$ of this ensemble can be written as

$$\begin{aligned} \exp[-\beta F] &= \sum_{N_p=0}^{\infty} \frac{z_p^{N_p}}{N_c!\Lambda_c^{3N_c}N_p!}\,\mathrm{Tr}_c\,\mathrm{Tr}_p\exp[-\beta H] \\ &= \frac{1}{N_c!\Lambda_c^{3N_c}}\,\mathrm{Tr}_c\exp[-\beta H^{\mathrm{eff}}], \end{aligned} \qquad \textbf{[S1]}$$

where the trace Tr_c is short for the volume integral $\int_V d\mathbf{R}^{N_c}$ $\int_\Omega d\hat{\omega}^{N_c}$ over the coordinates and orientations of the coated particles, and similarly $\mathrm{Tr}_p = \int_V d\mathbf{r}^{N_p}$. The effective Hamiltonian of the coated particles can be written as

$$H^{\mathrm{eff}} = H_{cc} - z_p V_f, \qquad \textbf{[S2]}$$

where $z_pV_f = z_pV_f(\{\mathbf{R}\}, \{\hat{\omega}\})$ is the negative of the grand potential of the fluid of ideal polymer coils in the static configuration of N_c coated colloids with coordinates $\{\mathbf{R}\}$ and orientations $\{\hat{\omega}\}$. Here $V_f(\{\mathbf{R}\}, \{\hat{\omega}\})$ is the free volume of the polymers in the configuration of the colloids. Because of the ideal character of the polymer-polymer interactions it can be written explicitly as

$$V_f = \int_V d\mathbf{r}\exp\left[-\sum_{i=1}^{N_c}\beta\phi_{cp}(\mathbf{R}_i - \mathbf{r}, \hat{\omega}_i)\right]. \qquad \textbf{[S3]}$$

Non-vanishing contributions to V_f stem from those positions $\mathbf{r}$ that are outside any of the N_c depletion shells. The shape of the free volume is highly irregular and non-connected. We decompose V_f, formally, into zero-colloid, one-colloid, two-colloid contributions, etc., by expanding it in terms of the colloid-polymer Mayer-function $f(\mathbf{R}_i - \mathbf{r}, \hat{\omega})$, which for the present model equals -1 for $\xi(\mathbf{R}_i - \mathbf{r}, \hat{\omega}) < 0$, and 0 otherwise. One finds

$$\begin{aligned} V_f &= \int_V d\mathbf{r}\prod_{i=1}^{N_c}(1 + f(\mathbf{R}_i - \mathbf{r}, \hat{\omega})) \\ &= V + \sum_{i=1}^{N_c} V_f^{(1)}(\mathbf{R}_i, \hat{\omega}_i) + \sum_{i<j}^{N_c} V_f^{(2)}(\mathbf{R}_i, \mathbf{R}_j, \hat{\omega}_i, \hat{\omega}_j) + \cdots \end{aligned} \qquad \textbf{[S4]}$$

For $k \geq 1$, the k-colloid contribution reads

$$V_f^{(k)} = \int_V d\mathbf{r}\prod_{m=1}^{k} f(\mathbf{R}_{i_m} - \mathbf{r}, \hat{\omega}_{i_m}), \qquad \textbf{[S5]}$$

where only those positions $\mathbf{r}$ give non-vanishing contributions where the depletion layers of (at least) k colloids overlap simultaneously.

We give explicit expressions for $V_f^{(k)}$ for $k = 1$ and 2 for equal-sized colloidal hard spheres with a smooth surface. It follows directly from Eq. **S4** that the one-body contribution $V_f^{(1)} = -v_1$ with $v_1 = \pi\sigma_{cp}^3/6$ and $\sigma_{cp} = (\sigma_r + \sigma_p)/2$, which can be interpreted as the volume that is excluded for a polymer coil by a single colloid. $V_f^{(2)}(\mathbf{R}_i, \mathbf{R}_j)$ is the lens-shaped overlap volume as depicted in Fig. 1*B* of two spheres of radius σ_{cp} at separation $R_{ij} = |\mathbf{R}_i - \mathbf{R}_j|$. We note that $-z_pV_f^{(2)}(R_{ij}) \equiv \beta\phi_{\mathrm{AO}}(R_{ij})$ is the well-known depletion potential of the AO model (6, 7), which was derived by Asakura and Oosawa as well as Vrij (8, 9). The effective pair potential $\phi_{\mathrm{eff}}(R_{ij}) = \phi_{\mathrm{cc}}(R_{ij}) + \phi_{\mathrm{AO}}(R_{ij})$ reads

$$\beta\phi(R_{ij}) = \begin{cases} \infty & \text{for } R_{ij} < \sigma_r \\ -\frac{\pi\sigma_p^3 z_p}{6}\frac{(1+q)^3}{q^3}\left[1 - \frac{3R_{ij}}{2(1+q)\sigma_r} + \frac{R_{ij}^3}{2(1+q)^3\sigma_r^3}\right] & \text{for } \sigma_r < R_{ij} < \sigma_r + \sigma_p\,. \\ 0 & \text{for } R_{ij} > \sigma_r + \sigma_p \end{cases}$$

This Asakura-Oosawa pair potential describes an attractive well close to the surface of the colloid, whose depth increases linearly with increasing z_p. The range of the potential is given by σ_p.

Similarly, we define an effective depletion potential for our coated spheres, which depends explicitly on the orientation of the coated spheres.

$$\begin{aligned} \beta\phi_{\mathrm{eff}}(\mathbf{R}_{ij}, \hat{\omega}_i, \hat{\omega}_j) &= \beta\phi_{\mathrm{cc}}(\mathbf{R}_{ij}, \hat{\omega}_i, \hat{\omega}_j) \\ &\quad - z_p\int_V d\mathbf{r} f(\mathbf{R}_i - \mathbf{r}, \hat{\omega}_i) f(\mathbf{R}_j - \mathbf{r}, \hat{\omega}_j). \end{aligned} \qquad \textbf{[S6]}$$

The three- and more-body contributions $V_f^{(k)}$ with $k \leq 3$ will be zero when the radius of gyration of the polymer coils is sufficiently small compared to the size of the colloids. The mapping of the full Hamiltonian of the colloid-polymer mixture can then be mapped exactly onto an effective Hamiltonian with only effective pairwise additive interactions, since three colloidal spheres cannot simultaneously overlap with a polymer coil. If the relaxation of the orientation degrees of freedom is much faster than that of the translational degrees of freedom, and the coated particles are sufficiently isotropic, we can perform a further coarse-graining by integrating out the orientational degrees of freedom of the effective interactions. The orientation-averaged effective pair potential reads

$$\beta\phi_{\mathrm{eff}}(R_{ij}) = -\log\left(\frac{1}{16\pi^2}\int_\Omega d\hat{\omega}_i \int_\Omega d\hat{\omega}_j \exp\left[-\beta\phi_{\mathrm{cc}}(\mathbf{R}_{ij},\hat{\omega}_i,\hat{\omega}_j) - z_p\int_V d\mathbf{r} f(\mathbf{R}_i-\mathbf{r},\hat{\omega}_i) f(\mathbf{R}_j-\mathbf{r},\hat{\omega}_j)\right]\right). \quad \textbf{[S7]}$$

Since the integrals over the orientations of the particles cannot be solved directly, we perform the orientation average by evaluating the integrand for many different random orientations. We have checked the convergence of our integrations.

In order to generate colloidal particles coated with small particles onto the surface, we perform Monte Carlo simulations of a binary mixture of oppositely charged particles in the *NVT* ensemble. The particles are assumed to interact with Yukawa interactions and we choose a negative charge on the small particles and a positive charge on the large particles. The charge magnitude was increased until all the small particles were attached onto the surface of the large particles. The structure of the small particles on the surface of the large particles can be tuned by the inverse screening length $\kappa\sigma_r$ in the Yukawa interaction of the particles. For low $\kappa\sigma_r$ the small particles are evenly distributed and very structured while for high $\kappa\sigma_r$ there is much more disorder in the coating of the small spheres. Using $\kappa\sigma_r = 10$, the resulting configurations gave the best match with the coated particles as employed in the experiments and as shown in Fig. 1*A*.

Once the two particles have been created they are placed next to each other in a cubic simulation box and 1×10^5 random orientations of the two particles are sampled. For the first 1000 non-overlapping configurations, we determine the effective pair potential. If non-overlapping configurations were found the particles are moved closer together and again orientations are generated and the potential calculated. To calculate the free volume we divide the space into cells. To calculate the overlap volume in each cell we first check whether the cell is completely embedded in the overlap volume or falls completely outside the overlap volume. If neither is the case the cell is divided into eight subcells for which we perform the same procedure. This is repeated until the volume of the cell is smaller than $1 \times 10^{-5}\sigma_r^3$, the algorithm then randomly generates ten points to estimate the overlap volume in this cell. The final overlap volume is than the sum of the overlap volumes of all cells. We tested the accuracy of this method for two spheres and the difference between the analytic expression and the calculation is less than $1 \times 10^{-5}\sigma_r^3$.

We calculated the effective pair potential for two rough spheres including the rough surface layer and the effective pair potential for a rough and a smooth sphere. The smooth spheres in this system have a diameter of $\sigma_s = 2.22$ μm, the rough spheres have a diameter of $\sigma_r = 2.92$ μm including the rough surface layer, the small spheres that form the roughness have a diameter of 185 nm and the polymers have diameters of 38 nm. In Fig. 1*C* we plot the effective pair potential between two smooth spheres, two rough spheres and one rough and one smooth sphere for a polymer reservoir density $\rho_p^r = 0.038\ \rho_{\mathrm{overlap}}$. We find significant attraction between the smooth spheres, while the attraction between a rough and a smooth sphere and between two rough spheres is negligible.

Direct simulations. We model the system as N asymmetric dumbbells consisting of a rough sphere and a smooth sphere in volume V with ideal polymer of density ρ_p and diameter σ_p. The diameters of the rough and smooth spheres are $\sigma_r = 2.92$ μm and $\sigma_s = 2.22$ μm, respectively. The effective pair potential for two smooth spheres is given by the Asakura-Oosawa depletion potential (6), where σ_r is replaced by σ_s and $q = \sigma_p/\sigma_s$ is the size ratio between the polymer and smooth spheres. The rough spheres are treated as hard spheres and the effective pair potential between rough and smooth spheres are assumed to be hard-sphere-like. We use Monte Carlo simulations in the canonical ensemble (NVT) to calculate the probability distribution of the cluster size $P(n) = N(n)/\Sigma_{n=1}^{n_{\max}} N(n)$, where $N(n)$ is the number of clusters of size n in a system containing $N = 1000$ dumbbells at a packing fraction of 0.003. To improve mobility of clusters containing more than one particle, cluster moves are introduced which collectively move all particles that are part of the same cluster. Particles are considered to be part of the same cluster if the distance between their smooth spheres is less than the attraction range $\sigma_s + \sigma_p$. Fig. S2 shows typical configurations of the MC simulations for two polymer sizes, $\sigma_p = 38$ and 16 nm. We clearly observe the formation of micelle-like clusters in addition to single dumbbell particles. The cluster size distributions are shown along with the experimental one in Fig. 3*C* for $\sigma_p = 38$ nm and in Fig. S6 for $\sigma_p = 16$ nm. Finally, we present typical configurations of the clusters containing $n = 1$ to $n = 15$ particles in Fig. 2 together with the experimental images.

Free energy calculations. The free energy of clusters of different sizes can be calculated using grand-canonical Monte Carlo (GCMC) simulations on single clusters. A similar method has previously been used to study the formation of micelles from surfactants (10). We model the particles in the same way as in the direct Monte Carlo simulations, and assume that the gas of clusters is sufficiently dilute to behave as an ideal gas. The partition function for the total system of clusters is then given by:

$$Q = \prod_{n=1}^{\infty} \frac{Q_n^{N_n}}{N_n!}, \quad \textbf{[S8]}$$

$$Q_n = \frac{1}{(4\pi)^n \Lambda^{3n} n!}\int_V d\mathbf{r}^n \int d\mathbf{n}^n \exp(-\beta U(\mathbf{r}^n,\mathbf{n}^n)) h(\mathbf{r}^n,\mathbf{n}^n), \quad \textbf{[S9]}$$

where N_n is the number of clusters of size n, Λ is the coarse-grained length scale (e.g. in atomic systems the De Broglie wavelength), $\beta = 1/k_{\mathrm{B}}T$, and $\mathbf{r}^n$ and $\mathbf{n}^n$ denote the positions and orientations of the dumbbell particles, respectively. The function $h(\mathbf{r}^n,\mathbf{n}^n)$ equals 1 if the particles with centers $\mathbf{r}^n$ and orientations $\mathbf{n}^n$ form a single cluster, and 0 otherwise. For an ideal gas of these particles, with only clusters of size 1, this yields the ideal gas free energy $\beta F/N = \log\rho\Lambda^3 - 1$. The partition function can also be written as:

$$Q = \prod_{n=1}^{\infty} \frac{(V/\Lambda^3)^{N_n}}{N_n!}\left(\frac{Q_n}{Q_1}\right)^{N_n}. \quad \textbf{[S10]}$$

Here, Q_n/Q_1 is the ratio of the partition function of a cluster of n particles to that of a cluster of one particle. This ratio can be measured from a grand-canonical Monte Carlo simulation, at fixed chemical potential μ. In a GCMC with the additional constraint that all particles should form a single cluster, the probability $P(n)$ of observing a cluster of size n obeys:

$$\frac{P(n)}{P(1)} = \exp[\beta\mu(n-1)]\frac{Q_n}{Q_1}. \quad \textbf{[S11]}$$

Hence, the ratios Q_n/Q_1 can be directly obtained from the GCMC simulations. These ratios are independent of μ, although simulations at different values of μ can be employed to sample all cluster sizes.

To find the cluster distribution of a system with an overall particle density ρ, we simply minimize the free energy $F = -k_{\mathrm{B}}T \log Q$ with respect to the number of clusters of each size. This yields:

$$\rho_n \Lambda^3 = (\rho_1 \Lambda^3)^n \exp(-\beta(f_n - f_1)), \qquad \textbf{[S12]}$$

with $f_n = -k_{\mathrm{B}}T \log(Q_n)$ the free energy of a cluster of size n. From this, it is straightforward to calculate the cluster size distribution for any overall system density. Note that the choice of Λ does not influence the results.

To measure the cluster free energies f_n, we simulate single clusters, and reject all moves that would break up this cluster. Apart from translation and rotation moves, we insert and remove particles according to a standard GCMC scheme, again restricting the system to single clusters. The box volume has no influence on the outcome of the simulation, as insertions will only be accepted near the cluster. In fact, only insertions inside the attractive wells of existing particles can be accepted without resulting in two separate clusters, so only insertion moves inside those wells are attempted. The volume in the normal acceptance rule for a GCMC insertion move is then replaced by the volume of n spherical shells with the size of the attractive well, where n is the number of particles in the system. As the potential wells of multiple particles can overlap, a correction is required to satisfy detailed balance when a particle is inserted into the attractive well of more than one neighboring particles. After normal acceptance, the move is only accepted with a probability of $1/k$, where k is the number of overlapping wells at the point of insertion.

To calculate the cluster size distributions, the free energy of a range of cluster sizes is needed. As the resulting cluster size can be very sensitive to the chemical potential, it is more convenient to set $\mu = 0$, and to implement a standard Umbrella Sampling scheme to sample the required cluster sizes instead. To improve sampling speed at high interaction strengths, we use parallel tempering. Each simulation contains a number of separate clusters, each at a different interaction strength, but biased towards the same cluster size. While the different clusters do not interact, a new Monte Carlo move is introduced that swaps configurations of two different interaction strengths.

If the interactions are weak, the distributions obtained from free energy calculations closely match those from the direct simulations. However, when the interactions are strong enough that larger clusters are formed, the equilibrium distributions show a strong preference for specific cluster sizes much larger than those seen in the direct simulations (see Fig. S3). Clusters around size 10 are not found in significant quantities for any interaction strength. In particular, at the packing fraction and interaction range used in the experiments and the direct simulations, cluster sizes 19, 20, 22, and 23 all appear as common cluster sizes, depending on the polymer concentration. Figures of typical clusters of these sizes are shown in Fig. S4. These clusters all display a large number of bonds per particle, and the smooth spheres in the micelles show crystalline order, with a tetrahedral structure (marked in pink) at the center. Forming these clusters spontaneously would require a large number of reorganizations including breaking several bonds. As explained earlier, this will not happen within a reasonable time scale.

It is interesting to note that the cluster sizes preferred in these distributions do not always maximize the number of bonds per particle, which would minimize the potential energy of the cluster. For example, from the clusters of sizes 19, 20, 22, and 23 shown in Fig. S4, the lowest-energy cluster is size 22, with 6.545 bonds per particle, but this size is not particularly common in the distributions in Fig. S3. Clearly, entropic effects still need to be taken into account to predict what clusters will appear more often.

Supplementary Derivations. ***Interaction potential.*** The short ranged depletion attraction between the colloids is significantly lowered by the screened Coulomb repulsions. We take the attractive depletion potential to be Eq. **S6** and the screened Coulomb potential to be:(11)

$$u_{el}(x) = \frac{\Psi^2(\sigma_s/2)^2}{\lambda_B x} \exp[-\kappa(x - \sigma_s)], \qquad \textbf{[S13]}$$

where σ_s is the diameter of the smooth side of the colloids, $\Psi = 0.6\ k_{\mathrm{B}}T$ is the zetapotential of the particles measured by laser doppler electrophoresis, $\lambda_B = 0.71$ nm is the Bjerrum length in water, and κ is the inverse of the Debye screening length, and x is the distance between the centers of the two particles. At 20 mM NaCl, $\kappa \approx 0.5\ \mathrm{nm}^{-1}$. The Asakura-Oosawa potential (AO) is plotted together with the screened Coulomb repulsion (C) in Fig. S5. For polymer concentrations at which clustering was observed, the minimum of the total potential (tot) is roughly $-5\ k_{\mathrm{B}}T$ for the polymer with 8 nm radius (Fig. S5*A*), and $-17\ k_{\mathrm{B}}T$ for polymer with 19 nm radius (Fig. S5*B*). Clearly, screened Coulomb repulsion significantly reduces the short-ranged depletion potential. However, the actual value for the interaction strength may be different as the minimum of the potential energy strongly depends on value of the zetapotential, namely as $u_{el} \propto \Psi^2$. The error associated with measuring the zetapotential on anisotropic particles thus makes the values obtained from screened Coulomb potentials approximative.

Escape rate for a single particle from a cluster. A particle diffusing in an energy potential well $u(x)$ with x the distance to closest approach and minimum at position b can escape that well with rate $r = \tau^{-1}$. We numerically calculate the escape time τ using Kramer's approach (12):

$$\tau = \int_a^c \mathrm{e}^{-u(x)/k_{\mathrm{B}}T} \mathrm{d}x \int_b^e \frac{1}{D(y)} \mathrm{e}^{u(y)/k_{\mathrm{B}}T} \mathrm{d}y. \qquad \textbf{[S14]}$$

Because the interaction range and thus the separation between interacting particles is short compared to the particle diameter, the problem is essentially one-dimensional. Here, $D(y)$ is the effective colloid diffusion constant in the well, which depends on the separation y between the colloids due to lubrication effects as: (13)

$$D(y) = \frac{8y}{\sigma_s} D_0, \qquad \textbf{[S15]}$$

D_0 is the diffusion constant for an unperturbed particle and can be calculated from the Einstein relation. Given the parameters in our system, where we estimated the viscosity to be $\eta = 2$ mPa·s (14), the diffusion constant D_0 is roughly $1 \cdot 10^{-13}\ \mathrm{m}^2/\mathrm{s}$.

We integrated the total potential as shown in Fig. S5 numerically for different numbers of bonds. To compare the results with the experimental values for the escape times, we scale the energy axis such that the minimum for one bond corresponds to $-10\ k_{\mathrm{B}}T$ as was deduced from the simulations. We chose the values for the integration boundaries as follows: $a = 5$ nm and $c = 20$ nm. The precise values of a and c are arbitrary but irrelevant. The minimum b is located at 10 nm, where again the precise value is not critical. However, the result depends fairly strongly on the choice of the upper integration limit e, see Eq. **S14**, which is the point were we consider the particle to have escaped from the dimer. Experimentally the particle must have traveled a few hundred nanometers before the observer decides whether the particle has escaped. Therefore, a natural choice for this boundary is a few hundred nanometers. Here we took $e = 400$ nm. With this input the escape time from a dimer is found to be 630 s. This result seems consistent with direct observations from light microscopy, where typically 10 min is observed for a particle to escape from a dimer. For comparison, the theoretical time to reach a hypothetical escape at $d = 38$ nm, which is the range of the potential, is 54 s. For the observer, the particle has not escaped yet, even if it is outside the influence of the potential, because it still has a large chance to diffuse back into the trap without the observer noticing it had 'escaped'.

If we calculate the escape time to break two bonds with the escape distance being located at 400 nm we find 95 days. To break three bonds it takes 4000 years according to these calculations and to break five bonds about $1 \cdot 10^{12}$ years. These long lifetimes for more than one bond are consistent with the fact that we have not observed such events in our experiments.

Supplementary experiments. Besides the experiments with dextran polymer of $r_p = 19$ nm as depletant, we also employed a smaller sized dextran polymer $r_p = 8.9$ nm in size. Fig. S6 shows transmission light micrographs of samples at increasing polymer concentration. At a polymer concentration of $\rho_p = 0.16\rho_{\text{overlap}}$, the depletion potential is insufficient to cause aggregation between the colloidal particles. A slightly higher polymer concentration of $\rho_p = 0.19\rho_{\text{overlap}}$ induces attractions between the smooth, small sides of the colloidal particles, leading to small clusters of $n = 1$ to $n = 4$ colloids in size. Above polymer concentrations of $\rho_p = 0.22\rho_{\text{overlap}}$ formation of colloidal clusters with the attractive and smooth sides of the dumbbells at the inside occurs. All data shown was taken after 9 days. The distributions for $\rho_p = 0.16\rho_{\text{overlap}}$ and $\rho_p = 0.19\rho_{\text{overlap}}$ did not evolve anymore after 1 day, the distribution for $\rho_p = 0.22\rho_{\text{overlap}}$ did not evolve significantly anymore after a few days. Qualitatively this aggregation behavior is comparable to the observations on the larger depletant as shown in Fig. 3 of the manuscript. Quantitatively, there are differences in the agreement of the cluster size distributions of the experiments and simulations as shown in Fig. S6. Clearly, only a weak agreement is obtained, with experiments showing a wide range of clusters sizes in contrast to the peak found in simulations. The range of the depletion potential is roughly the diameter of the depletant, and thus, for the smaller polymer shorter by more than a factor 2 compared to the larger polymer. Within these short-ranged attractive potentials rearrangement of the clusters is difficult and equilibration experimentally not achievable within a reasonable time-scale. Estimates of the added screened Coulomb-interaction and depletion interactions also indicate a deeper minimum compared to the larger polymer. The shorter interaction range and the stronger maximum attraction are likely the cause for the increased equilibration times.

1. Kim J-W, Larsen R, Weitz DA (2006) Synthesis of nonspherical colloidal particles with anisotropic properties. *J Am Chem Soc* 128:14374–14377.
2. Sheu H, El-Aasser MS, Vanderhoff J (1990) Phase-separation in polystyrene latex interpenetrating polymer networks. *J Polym Sci Part A: Polym Chem* 28:629–651.
3. Kegel WK, Breed D, Elsesser M, Pine DJ (2006) Formation of anisotropic polymer colloids by disparate relaxation times. *Langmuir* 22:7135–7136.
4. Badaire S, Cottin-Bizonne C, Woody J, Yang A, Stroock A (2007) Shape selectivity in the assembly of lithographically designed colloidal particles. *J Am Chem Soc* 129:40–41.
5. Dijkstra M, Brader JM, Evans R (1999) Phase behaviour and structure of model colloid-polymer mixtures. *J Phys: Condens Matt* 11:10079–10106.
6. Vrij A (1976) Polymers at interfaces and the interactions in colloidal dispersions. *Pure Appl Chem* 48:471–483.
7. Gast AP, Hall CK, Russel WB (1983) Polymer-induced phase separations in nonaqueous colloidal suspensions. *J Colloid Interface Sci* 96:251–267.
8. Asakura S, Oosawa F (1954) On interaction between two bodies immersed in a solution of macromolecules. *J Chem Phys* 22:1255–1256.
9. Asakura S, Oosawa F (1958) Interaction between particles suspended in solutions of macromolecules. *J Polym Sci* 33:183–192.
10. Pool R, Bolhuis PG (2005) Acurate free energies of micelle formation. *J Phys Chem B* 109:6650–6657.
11. Verwey EJW, Overbeek JThG (1948) *Theory of the Stability of Lyophobic Colloids* (Elsevier, New York).
12. Kramers HA (1940) Brownian motion in a field of force and the diffusion model of chemical reactions. *Physica* 7:284–304.
13. Russel WB, Saville DA, Schowalter WA (1991) *Colloidal Dispersions*, (Cambridge Univ Press, Cambridge, UK), Chapter 2.8.
14. Gündüz U (1996) Evaluation of viscosities of polymer-water solutions used in aqueous two-phase systems. *J Chromatogr B: Anal Technol Biomed Life Sci* 6880:263–266.

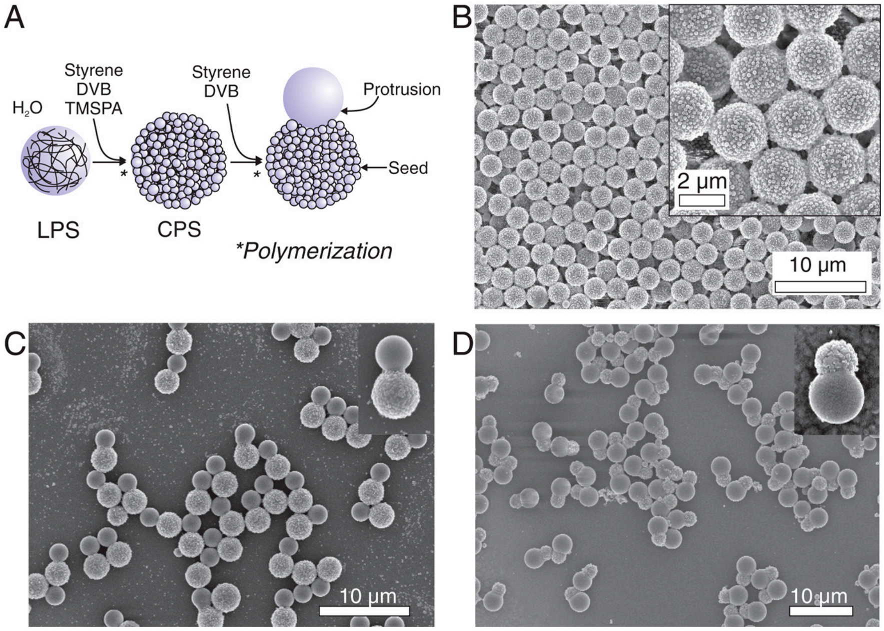

Fig. S1. Schematic synthesis of patchy particles. (*A*) Linear polystyrene (LPS) spheres are crosslinked by swelling with an emulsion consisting of styrene, divinylbenzene (DVB), and 3-(trimethoxysilyl)propyl acrylate (TMSPA). During polymerization, secondary nucleated particles render the particle surface rough by adsorption. SEM image of the rough spheres is shown in *B*. A second swelling step with an emulsion consisting of styrene and DVB yields rough particles with a smooth protrusion, as shown in *C*. (*D*) Transmission light micrograph of the particles in *C*. (*E*) SEM image of particles with smooth protrusions larger than the rough seed particles.

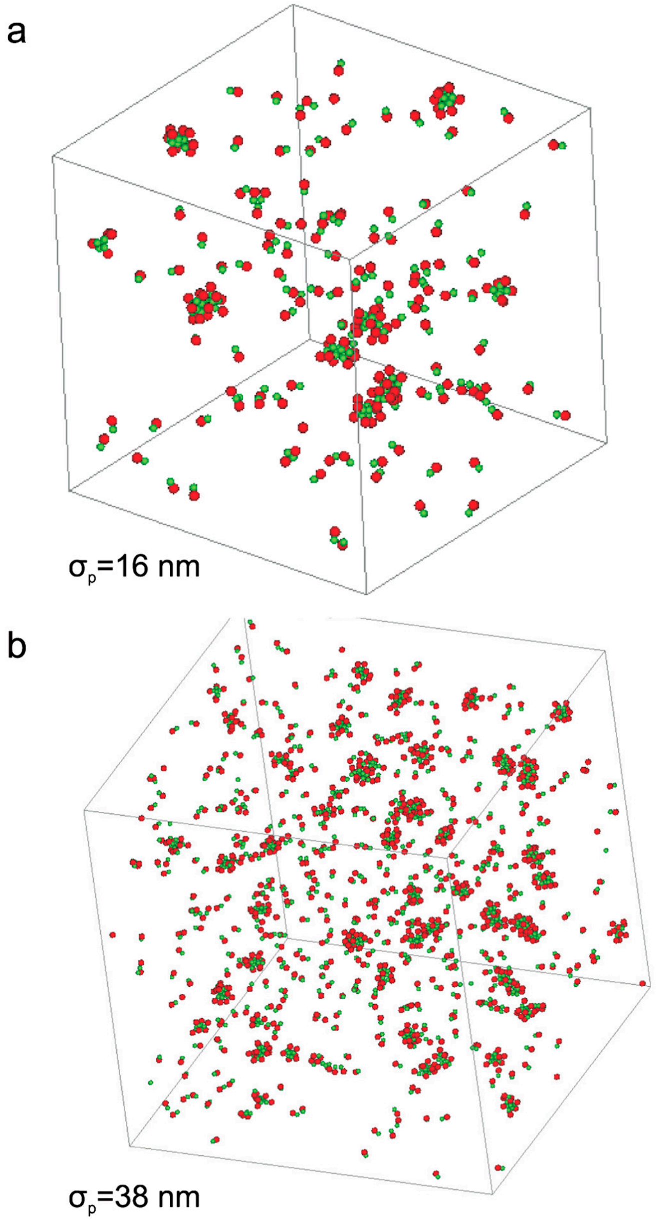

Fig. S2. Snapshots of Monte Carlo simulations after 10^8 MC cycles performed on dimers with one attractive sphere (green) and one hard sphere (red) modeled after the experimentally employed colloids. An attractive Asakura-Oosawa-Vrij potential between the green spheres of the dimers is induced by the addition of polymers with a diameter (*A*) $\sigma_p = 16$ nm, and (*B*) $\sigma_p = 38$ nm. Micelle-like clusters are visible next to single colloids.

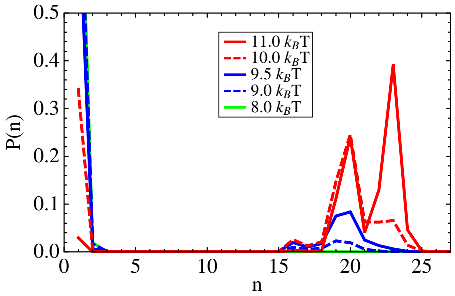

Fig. S3. Equilibrium cluster size distributions of dumbbells consisting of a rough and a smooth sphere with size ratio $\sigma_s/\sigma_r = 0.76$ at various interaction strengths (contact value ranging from 8 to 11 k_BT), using the experimental packing fraction $\eta = 0.003$ and polymer size $\sigma_p/\sigma_s = 0.02$.

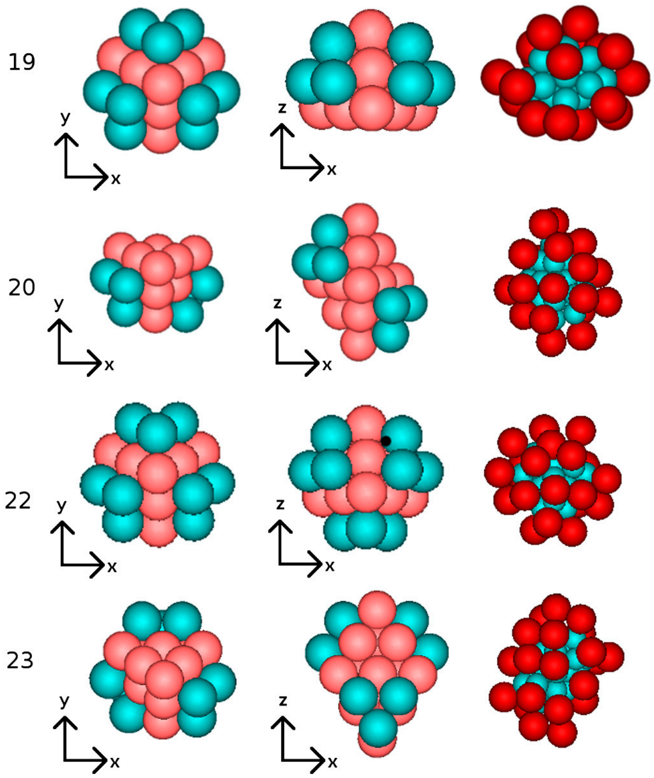

Fig. S4. Typical clusters of common sizes in the equilibrium distributions. For each size, two snapshots are shown where the rough spheres are removed, and one with the rough spheres included.

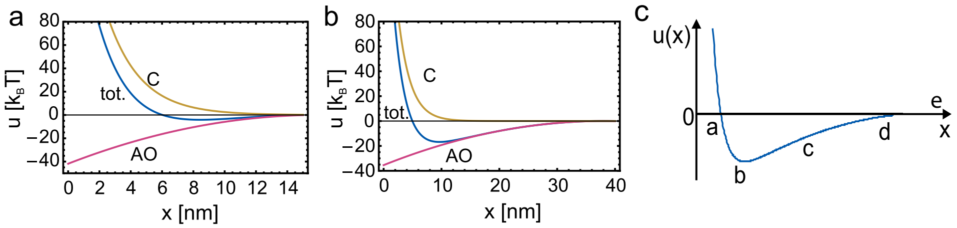

Fig. S5. A short-ranged screened Coulomb repulsion (C) reduces the Asakura-Oosawa (AO) depletion potential considerably, yielding an overall potential (tot) with a much smaller absolute minimum energy. Potential energies are plotted as a function of the distance x between surfaces of the two spheres. (*A*) Shows the potentials for $r_p = 8.9$ nm and $\rho_p = 0.2\rho_{\text{overlap}}$, and (*B*) for $r_p = 19$ nm and $\rho_p = 0.4\rho_{\text{overlap}}$. (*C*) Schematic interaction potential to illustrate the integration boundaries used to calculate the Kramer's escape time.

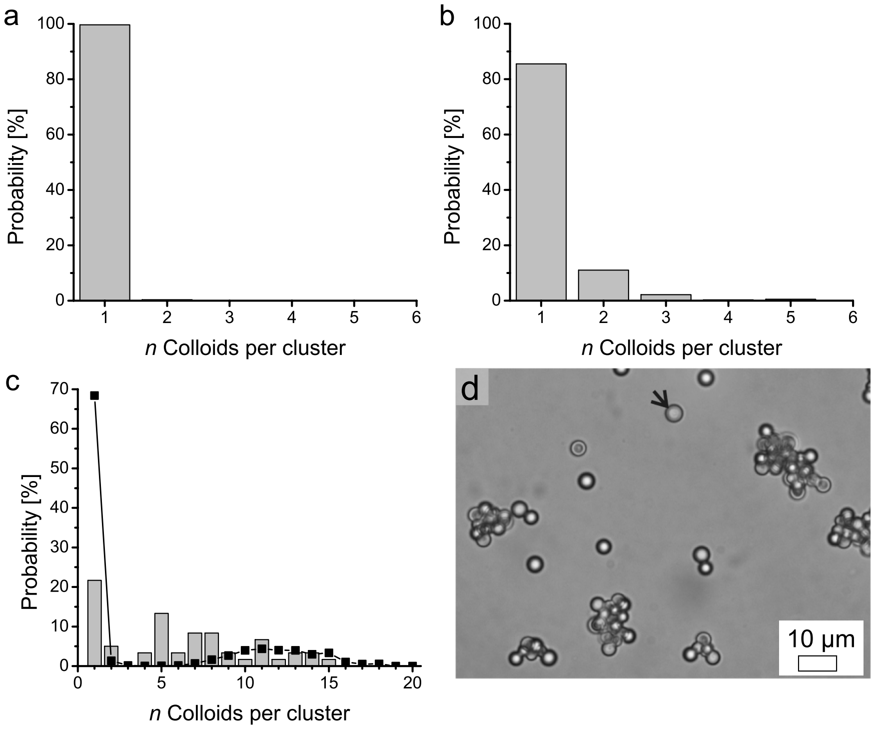

Fig. S6. Cluster size distributions for experiments (bars) and simulations (symbol and line) for dextran polymer with radius $r_p = 8$ nm at concentrations (*A*) $\rho_p = 0.16\rho_{\text{overlap}}$, (*B*) $\rho_p = 0.19\rho_{\text{overlap}}$ and (*C*) $\rho_p = 0.22\rho_{\text{overlap}}$. The experimental cluster size distribution in *C* ranges from $n = 5$ to $n = 15$, whereas simulations show a peak at $n = 10$, probably induced by the long experimental equilibration time due to the short-ranged interactions. (*D*) Transmission light micrograph of sample *C* with $\rho_p = 0.22\rho_{\text{overlap}}$. Data taken 9 d after sample preparation.

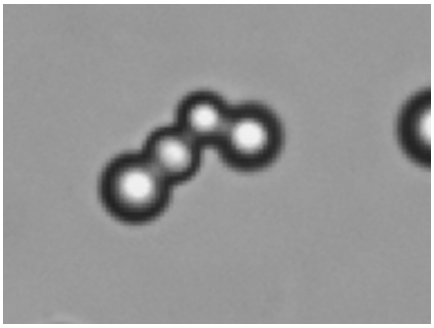

Movie S1. This movie file shows the spontaneous unbinding and binding between two colloids consisting each of one larger rough and one smaller smooth sphere in the presence of polymer ($\rho_p(r = 19 \text{ nm}) = 0.38\rho_{\text{overlap}}$). Note that after several binding attempts a bond between the colloids is only established at the end of the movie. The movie was acquired at 30 fr/s and it is displayed at 60 fr/s. (Quicktime, 5 MB)

Movie S1 (MOV)

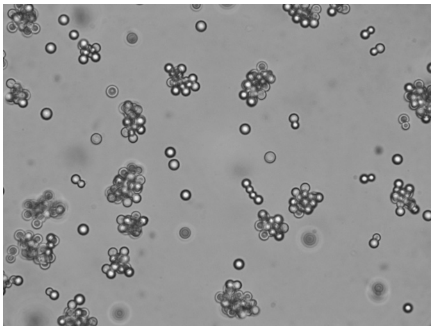

Movie S2. This movie file shows a self-assembled colloidal micelle-like cluster. The colloidal particles assemble in the presence of depletion attraction with their smooth and attractive sides at the interior of the clusters, whereas the rough, non-attractive sides are located at the outside. Despite its larger size, a rough sphere does not take part in the cluster as it does not have a smooth surface. Polymer concentration is $\rho_p(r = 19\ \mathrm{nm}) = 0.38\rho_{\mathrm{overlap}}$. The movie was acquired at 30 fr/s and it is displayed at 30 fr/s (Quicktime, 5 MB)

Movie S2 (MOV)

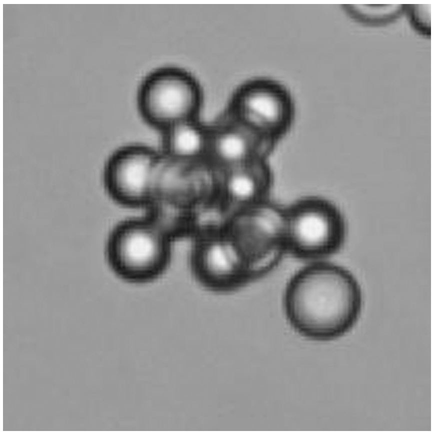

Movie S3. This movie file shows a typical, randomly selected full field of view of our sample containing free colloids as well as colloidal micelles. Polymer concentration is $\rho_p(r = 19\ \mathrm{nm}) = 0.38\rho_{\mathrm{overlap}}$. The movie was acquired at 30 fr/s and it is displayed at 60 fr/s (Quicktime, 2.1 MB)

Movie S3 (MOV)